Supplementary information

For

Binding Thermodynamics of (E)-2-((2-hydroxybenzylidene)amino)-5-methylbenzonitrile and (E)-2-((2-hydroxybenzylidene)amino)-5-methylbenzonitrile Cobalt(II) with HSA an Experimental and Molecular Dynamic Study

Sheldon Sookai[a,*], Ibrahim Waziri[b], Alfred J. Muller[b], and Monika Nowakowska[a]

[a]Molecular Sciences Institute, School of Chemistry, University of the Witwatersrand, PO WITS 2050, Johannesburg, South Africa.

[b]Research Centre for Synthesis and Catalysis, Department of Chemical Sciences, University of Johannesburg, Johannesburg, South Africa.

[c]*Electronic Supplementary Information (ESI) available: Complete experimental details*

[*]*Corresponding authors:* Sheldon.Sookai@wits.ac.za, Monika.Nowakowska@wits.ac.za

Experimental

Reagents and instruments

The chemical materials and reagents employed in this study were procured from Merck Life Sciences (Pty) Ltd and were utilized without pre-purification. These included salicylaldehyde, 2-amino-5-methylbenzonitrile, cobalt(II) acetate tetra hydrate, dichloromethane, and methanol. To characterize and elucidate the structures of the synthesized compounds, various spectroscopic techniques were employed, including ^{1}H and ^{13}C NMR, FTIR, UV-Vis, single crystal X-ray diffraction, mass spectrometry, and CHN elemental analysis. Buffer reagents included potassium hydroxide (≥ 90%) flakes and potassium monobasic phosphate buffer (KH_2PO_4 ≥ 99 ACS) and were purchased from Sigma Aldrich, along with lyophilized HSA (≥ 97%) (fatty acid free).

Synthesis of HL and its complex, CoL

Synthesis of the ligand: (*E*)-2-((2-hydroxybenzylidene)amino)-5-methylbenzonitrile (HL)

The ligand was synthesized following established protocols [1]. In brief, a 20 mL methanol solution containing 2-hydroxybenzaldehyde1.00 g, 8.19 mmol, 1 eq) was combined with a 20 mL methanolic solution of 2-amino-5-methylbenzonitrile (1.08 g, 8.19 mmol, 1 eq), with the addition of three drops of formic acid. The mixture was stirred at room temperature for 3 hours, leading to the formation of a precipitate. The resulting solid was filtered, washed with ether, dried, and subjected to recrystallisation

in dichloromethane for purification. (**Scheme 1**) [1, 2]. Yield: 1.53 g (76.3 %); m.p.93 °C; ^{1}H NMR (500 MHz, DMSO-d_6): δ = 12.46 (s, 1H, OH), 9.10 (s, 1H, HC=N), 7.72 (t, 2H, *J* = 8.50 Hz, Ar-H), 7.68 (t, 1H, *J* = 8.0 Hz, Ar-H), 7.61 (d, 1H, *J* = 8.0 Hz, Ar-H), 7.49-7.45 (m, 1H, *J* = 8.5 Hz, Ar-H), 7.03-6.99 (m, 2H, *J* = 7.5 Hz, Ar-H), 2.37 (s, 3H, CH_3); ^{13}C NMR (125 MHz, DMSO-d_6): δ = 164.8, 160.2, 148.2, 137.3, 135.1, 134.1, 133.0, 132.7, 119.3, 119.0, 118.4, 117.0, 116.7, 107.7: (Ar-C), 20.0 (CH_3);IR_{ATR}: ν_{max}/cm^{-1}: 3200, 2224, 1645, 1340, 947, 750 cm^{-1}; UV (DMSO, 10^{-3} M): 215 and 308 nm; CHN Anal. Calc. for $C_{15}H_{12}N_2O$: C, 76.25; H, 5.12; N, 11.86; Expt.: C, 76.24; H, 5.12; N, 11.85; *m/z* $[M+H]^+$: Calc. for $C_{15}H_{12}N_2O$ = 237.1023; Found = 237.1149.

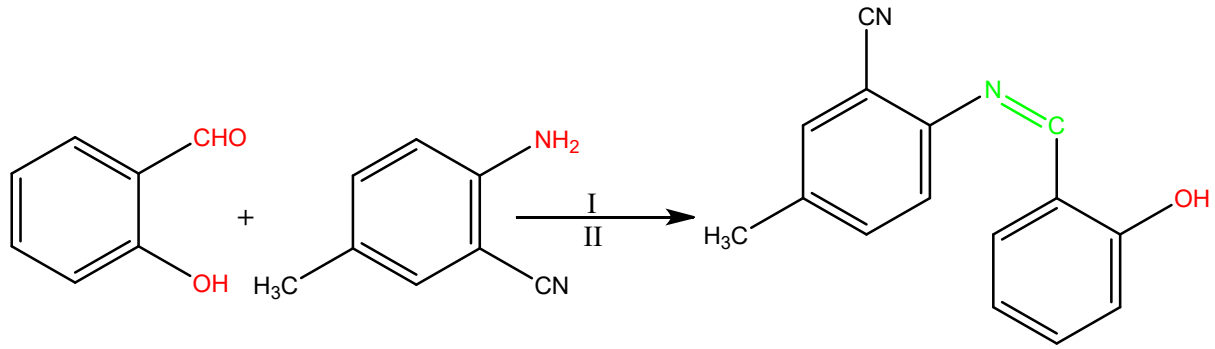

Scheme 1: Pathway for the synthesis of the ligand: (*E*)-2-((2-hydroxybenzylidene)amino)-5-methylbenzonitrile (HL); I = CH_3OH/HCOOH, II = RT, 3h

Synthesis of the complex: Bis (*E*)-2-((2-hydroxybenzylidene)amino)-5-methylbenzonitrile Cobalt(II) (CoL)

To a solution of the ligand, **HL** (0.35 g, 1.5 mmol, 2 eq) in 20 mL of dichloromethane was added a solution of $Co(OAc)_2{\cdot}4H_2O$ (0.19 g, 0.75 mmol) in 20 mL of methanol dropwise, after which the resulting mixture was stirred at room temperature for four hours. Thereafter, the precipitate form was filtered, washed with cold methanol (10×2 mL) and ether (10×2 mL) to afford the complex (**CoL)**. The reaction procedure is illustrated in **Scheme 2**.

Red solid; Yield: 65 %; m.p: 187-192 ^{o}C; UV-Vis:(DMSO, 10^{-3}M): λ_{max}/nm: 233 ($\pi\rightarrow\pi^*$), 348 ($n\rightarrow\pi^*$), 524 (d-d); IR_{ATR}: ν_{max}/cm^{-1}: 2215, 1600, 1458, 1389, 1189, 846, 743, 520, 463; CHN Anal. Calculated for $C_{30}H_{22}CoN_4O_2$; C, 68.06; H, 4.19; N, 10.58; Found: C, 68.05; H, 4.16; N, 10.55; HRMS-ESI *m/z* $[M]^+$: calculated for $C_{30}H_{22}CoN_4O_2$ = 529.1075; Found = 529.1086.

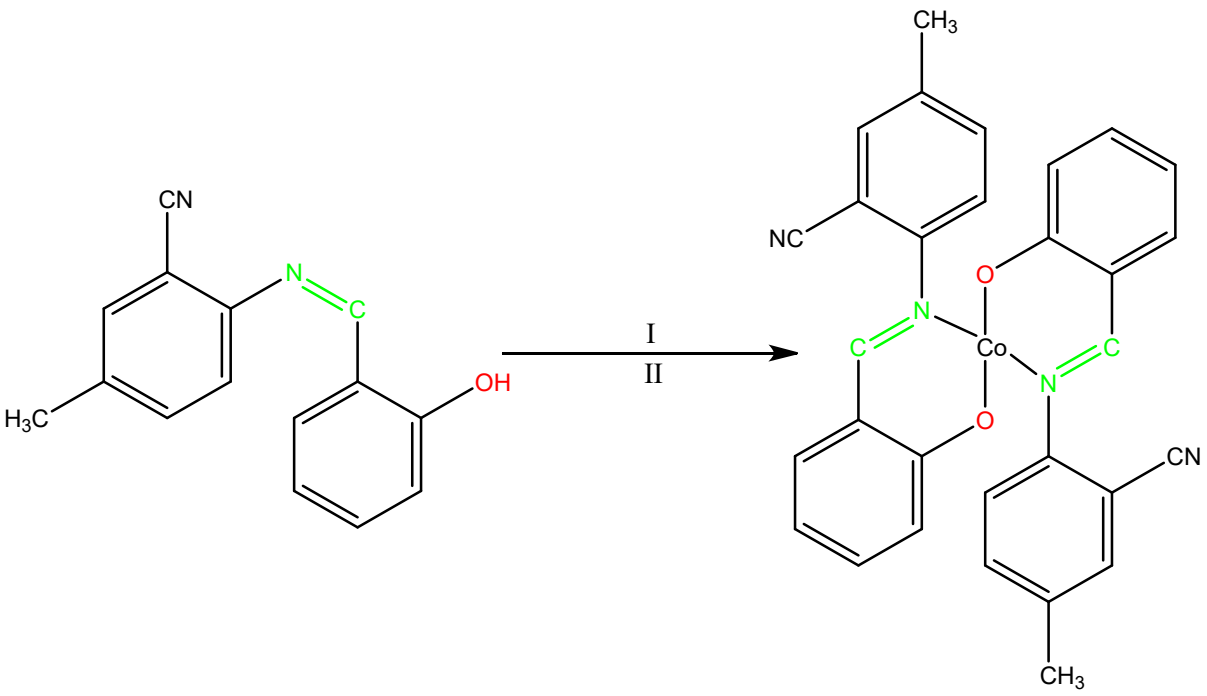

Scheme 2: Pathway for the synthesis of the complex: Bis (*E*)-2-((2-hydroxybenzylidene)amino)-5-methylbenzonitrile Cobalt(II) (CoL); I = $Co(OAc)_2.4H_2O$, II = CH_2Cl_2/CH_3OH, RT, 4h.

Spectra of the ligand (HL) and complex (CoL)

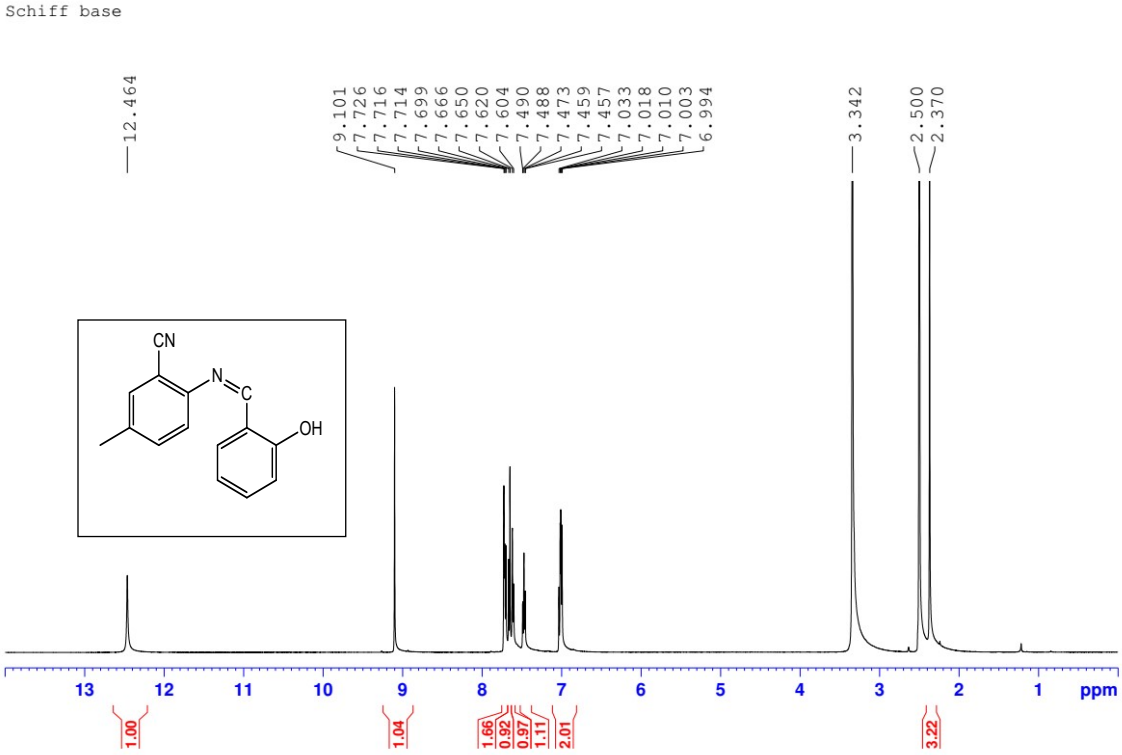

Figure S1: ^{1}H NMR spectrum of **HL** recorded at room temperature using (500 MHz, DMSO-d_6)

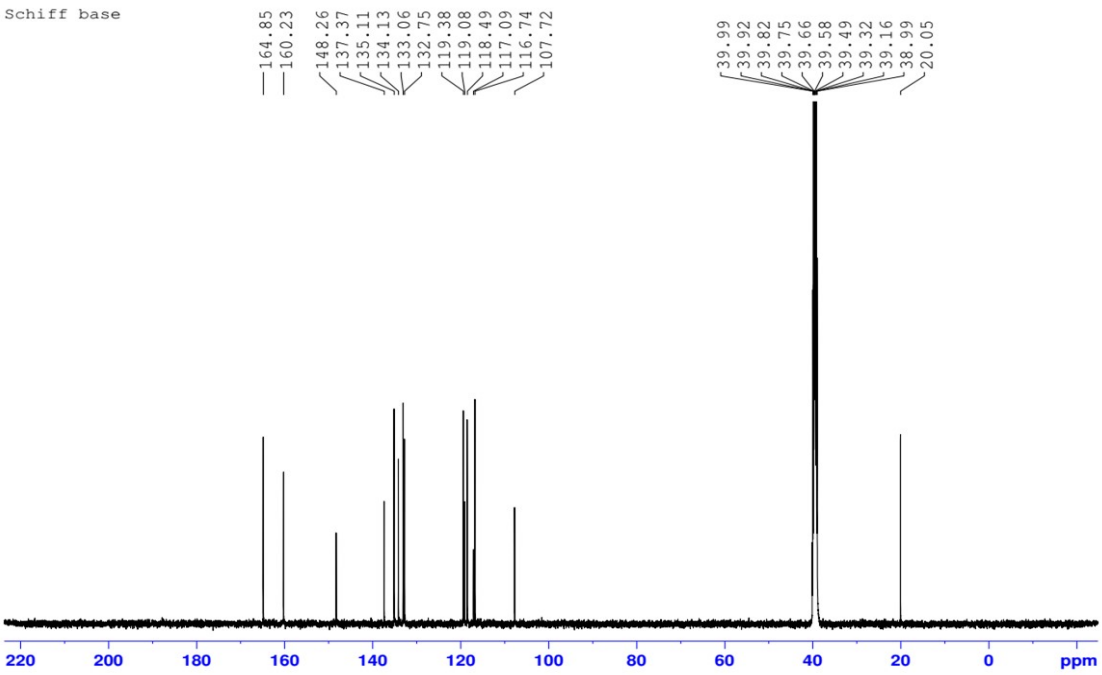

Figure S2: ^{13}C NMR spectrum of **HL** recorded at room temperature using (125 MHz, DMSO-d_6)

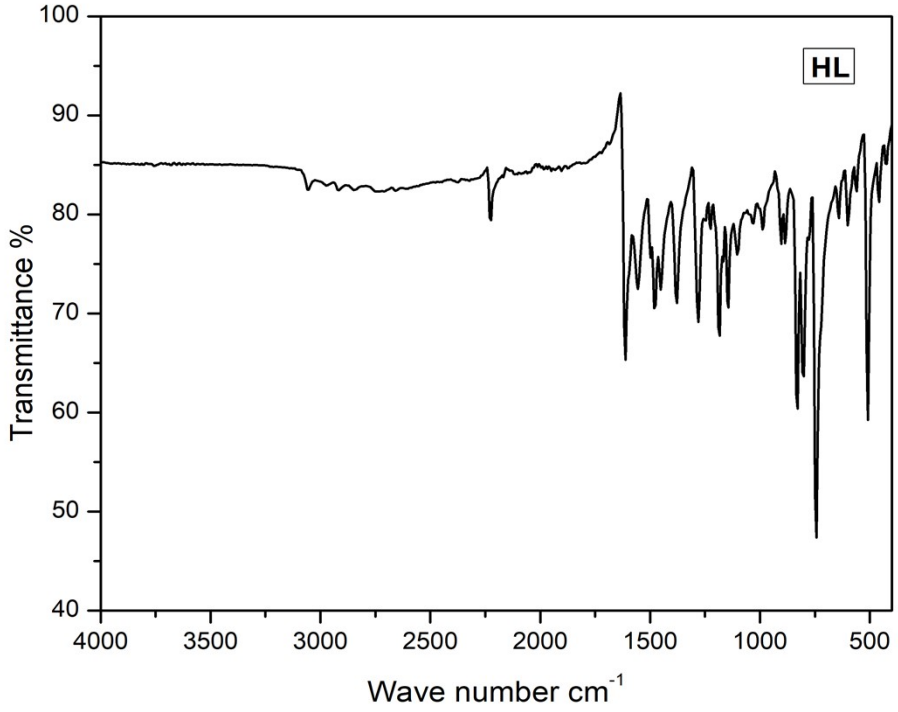

Figure S3: FTIR spectrum of **HL** obtained in solid state at room temperature using ATR method

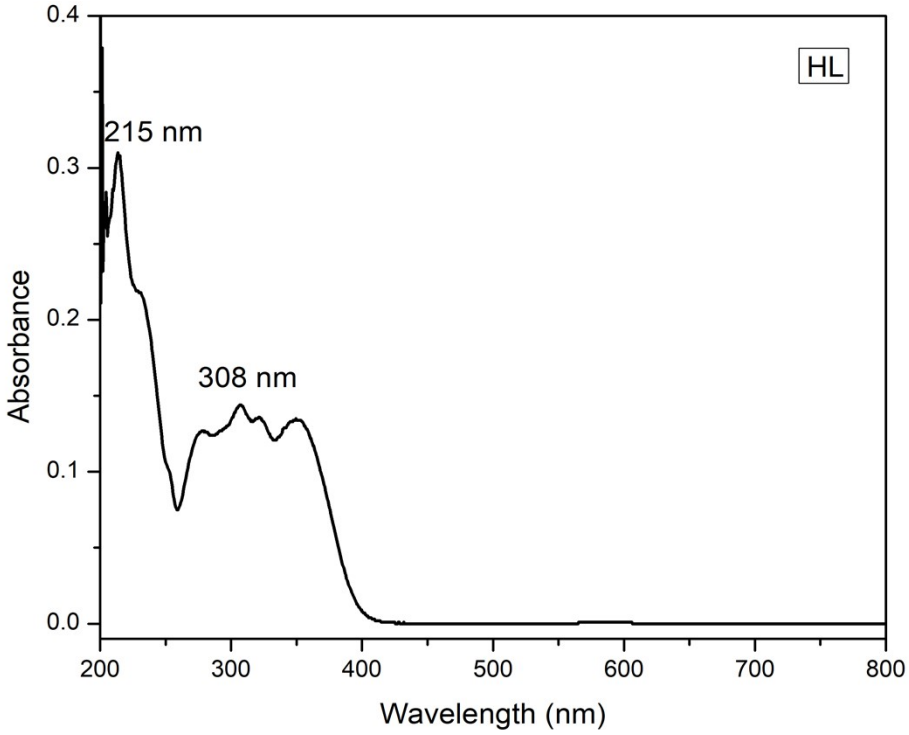

Figure S4: U-Vis spectrum of **HL** obtained at room temperature using (DMSO, 10^{-3}M)

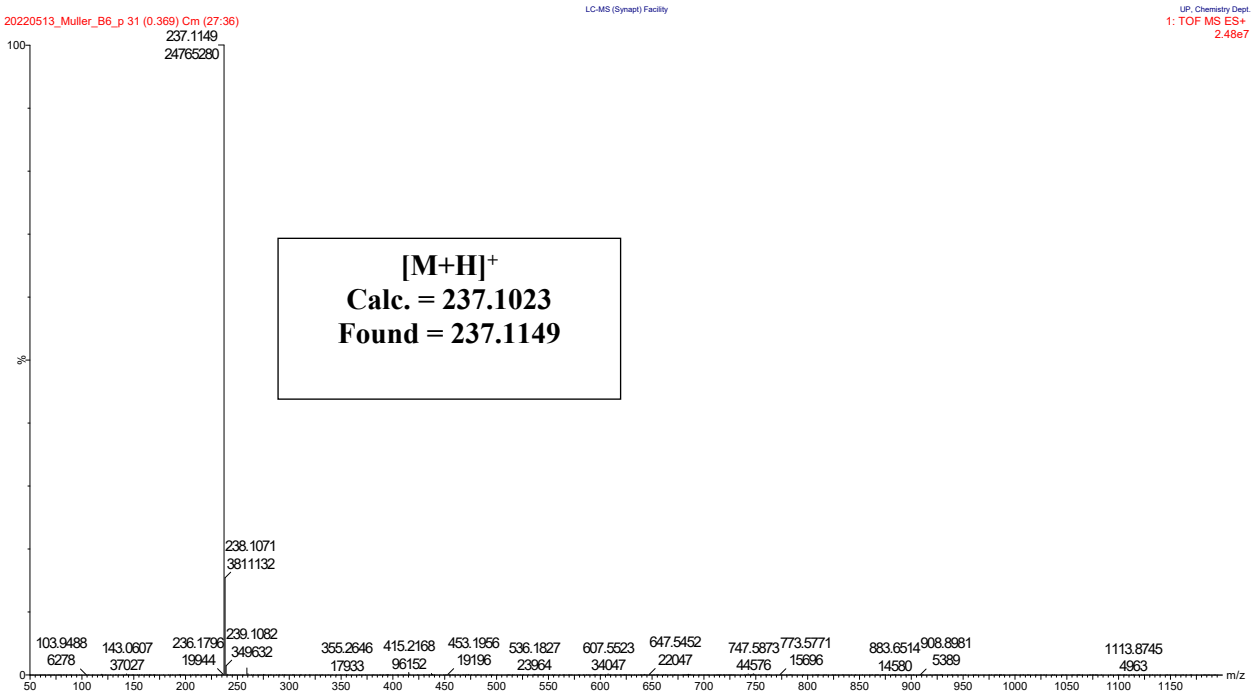

Figure S5: Mass spectrum of **HL** obtained using high resolution mass spectroscopy (HRMS)

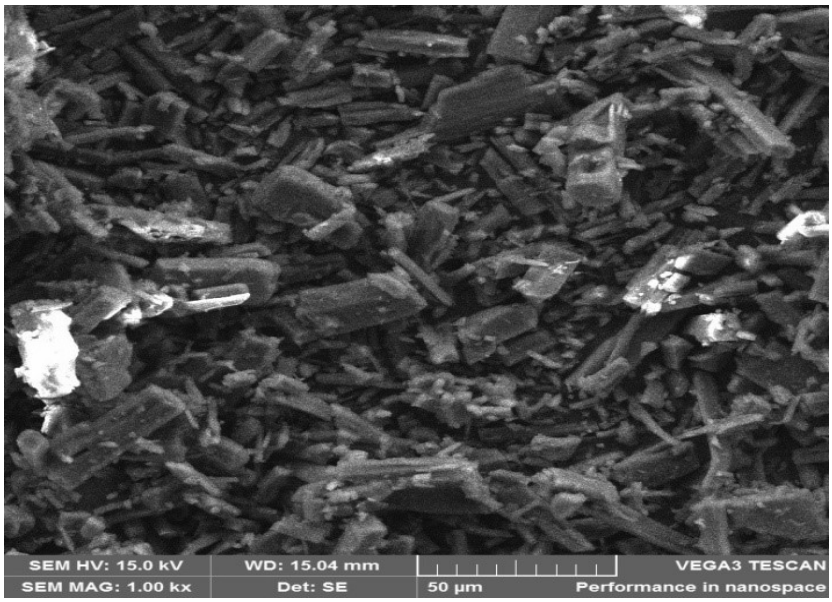

Figure S6: Scanning Electron Microscope (SEM) Image of **HL** shows block-like structures surface morphology in different forms and are well arranged, confirming the crystalline nature of the ligand. This was similar to previously reported structures

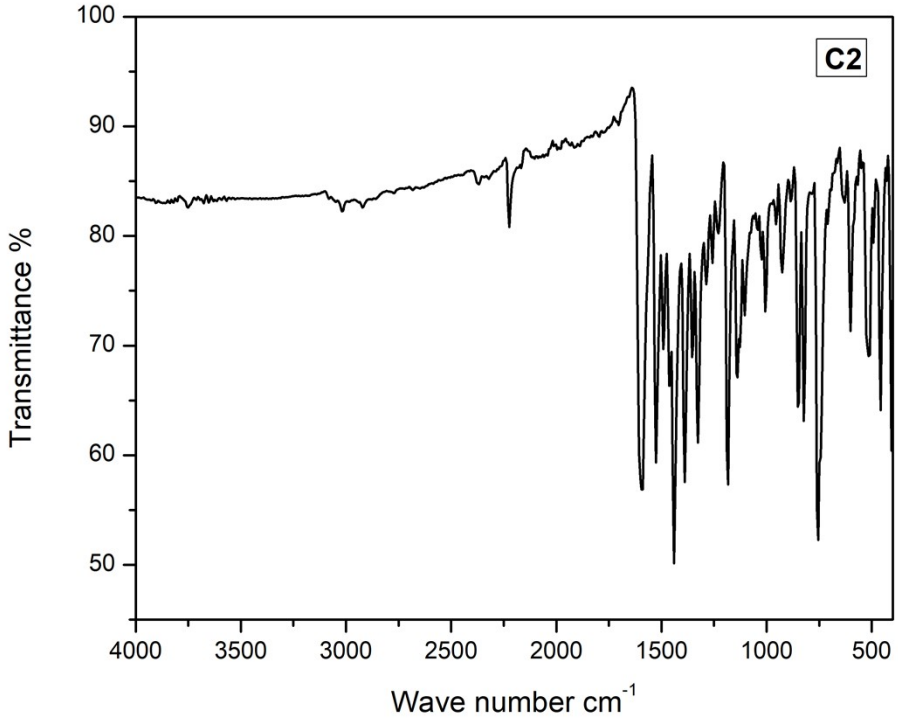

Figure S7: FTIR spectrum of **CoL** obtained in solid state at room temperature using ATR method

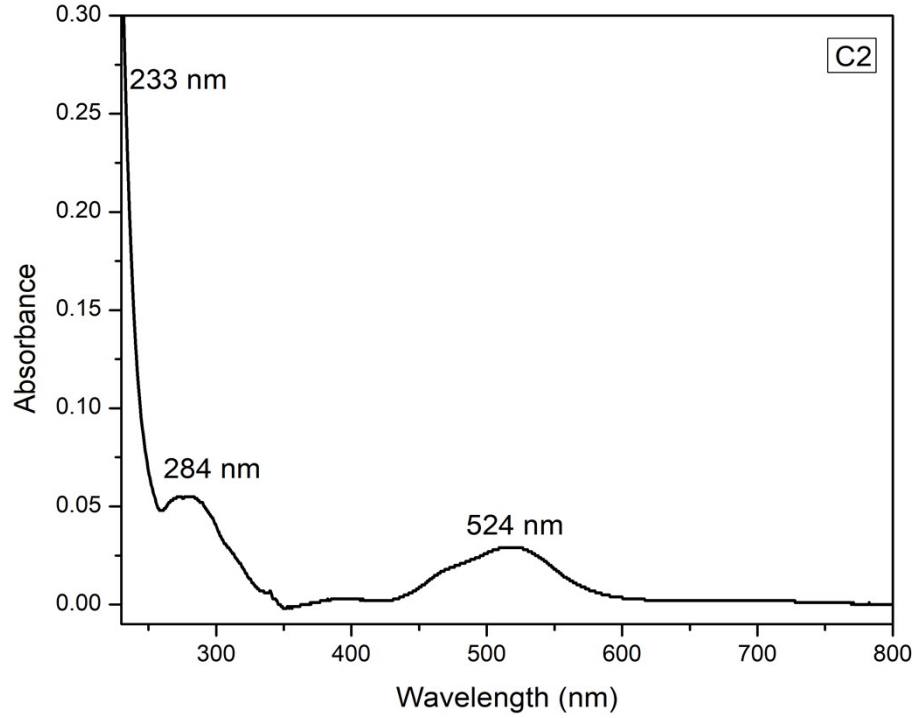

Figure S8: UV-Vis spectrum of **CoL** obtained at room temperature using (DMSO, 10^{-3} M)

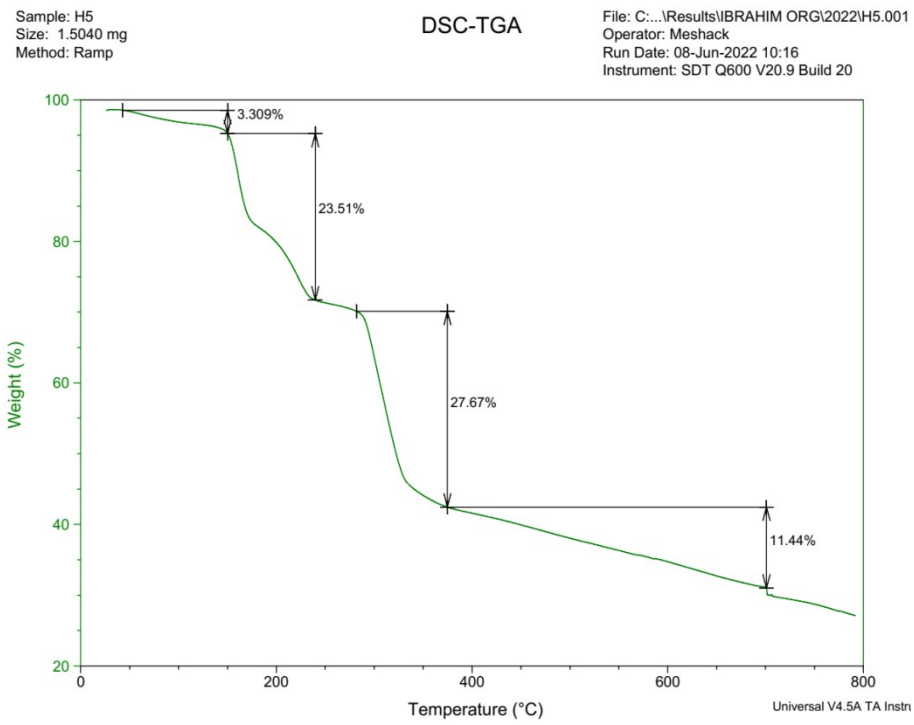

Figure S9: TGA Thermogram of **CoL** obtained under inert condition (N_2)

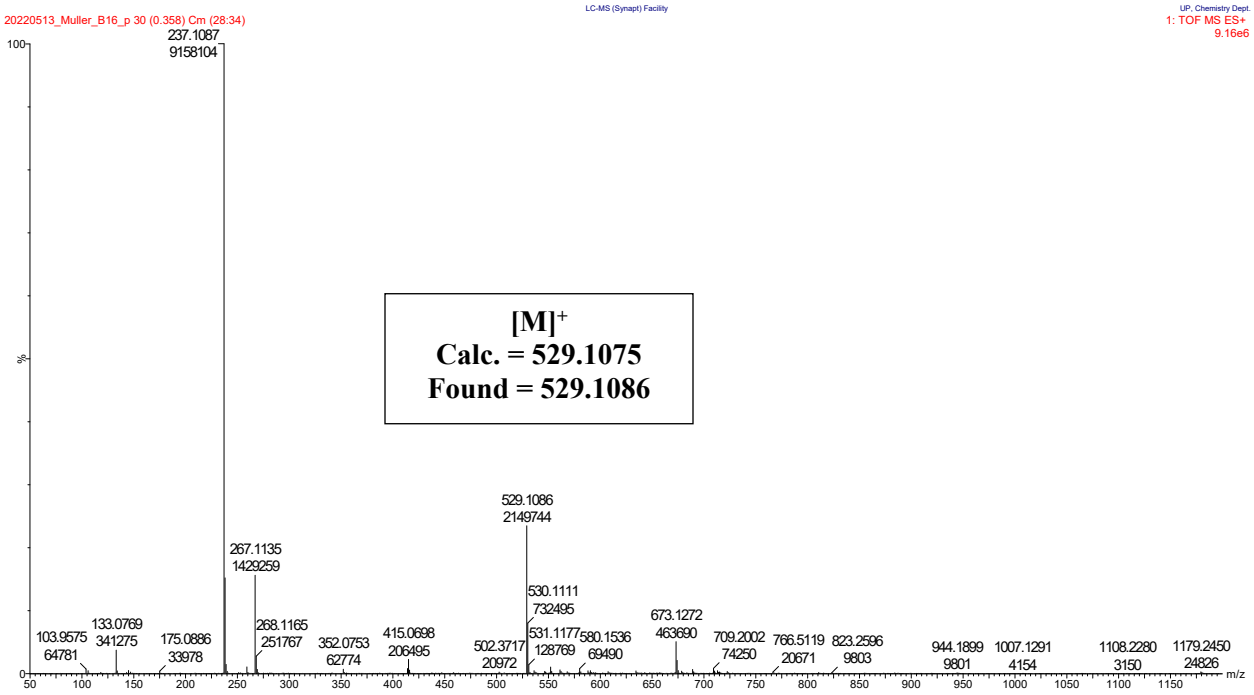

Figure S10: Mass spectrum of **CoL** obtained using high resolution mass spectroscopy (HRMS)

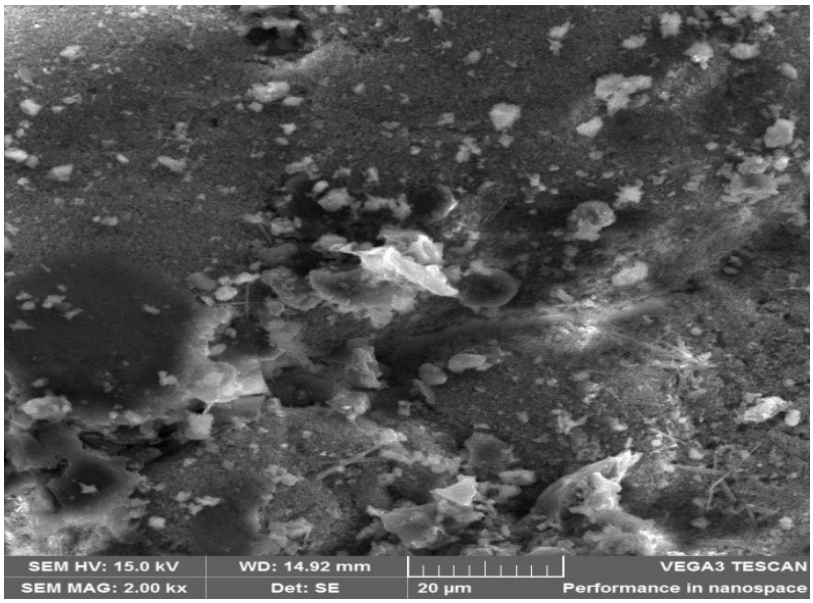

Figure S11: Scanning Electron Microscope (SEM) Image of **CoL**. SEM image of the ligand, HL (Figure S6) shows block-like structures surface morphology in different forms and are well arranged, confirming the crystalline nature of the ligand. But the complex's surface morphology here displayed a fine wide surface area with agglomeration of particles of different sizes and shapes scattered over it, indicating the amorphous nature of the complex. This change in the surface morphology of the ligand compared with the **CoL** herein confirmed the formation of new material (complex).

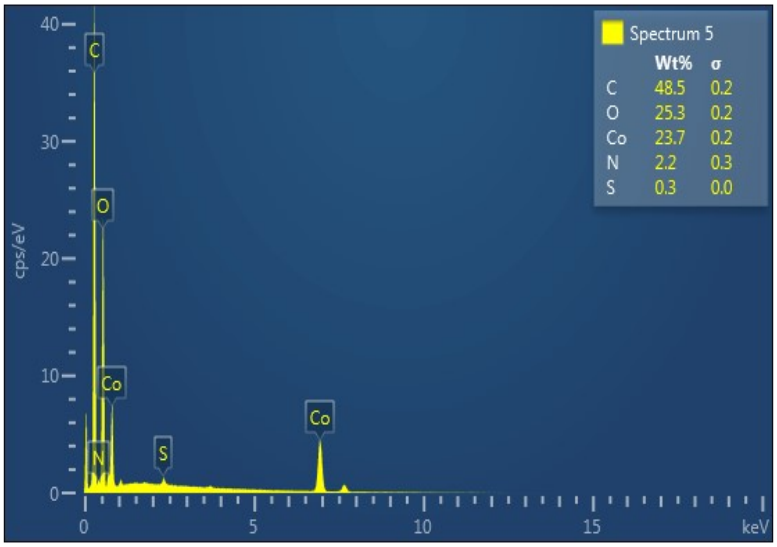

Figure S12: Energy Dispersive X-ray Spectroscopy (EDX) micrograph of **CoL** confirming the presence of Co(II) ion in the complex. In addition, carbon, nitrogen and oxygen atoms from the ligand were also confirmed. The presence of these elements within the compound has further affirmed the formation of the complex (**CoL**). The trace amount of sulfur (0.3%) could be due to impurity arising from coating of the sample.

Methods for Biophysical assays and *in silico* data

1.1. Fluorescence spectroscopy

Fluorescence measurements were performed in a similar manner to our previously reported methods[1]. In brief, fluorescence experiments were performed on a JASCO FP-8550 fluorescence spectrophotometer equipped with a Peltier temperature controller. The HSA concentration was kept at 3.0×10^{-6} mol dm^{-3} and the excitation and emission slit widths were fixed at 5 and 10 nm, respectively. The concentration of the ligands ranged from $0 – 48 \times 10^{-6}$ M. **HL** and **CoL** were dissolved in acetonitrile and the final acetonitrile concentration was under 5% (v/v) to prevent denaturation of HSA. The protein was excited at 295 nm (excitation of Trp-214), and the emission spectra were recorded from 310 to 450 nm. Spectral titrations were carried out at three temperatures (288, 298, and 310 K) in triplicate. HSA concentration was used at 3 μM to ensure significant protein intrinsic fluorescence. The ligand concentration was greater than 10 times the protein concentration in accordance to methods (i.e., eq. S2) [1].

Correction of fluorescence data. Inner filter effect (IFE) correction was applied to all fluorescence data using eq. S1[2],

$$F_{corrected} = F_{observed} * 10^{Aex * dex + Aem * dem} \quad \text{(S1)}$$

where $A_{excited}$ and $A_{emission}$ are the absorbance readings at the excitation and emission wavelengths, while d is the path length of the cuvette.

Fluorescent probe displacement assay. Warfarin and ibuprofen were used as specific site marker fluorescent probes for Sudlow's sites I and II, respectively. Steady-state fluorescence spectra were recorded as described above at 298 K using 5 nm excitation and emission bandwidths for warfarin, while 5 nm excitation and 5 nm emission band widths were employed for ibuprofen. The fluorophores warfarin and ibuprofen were equilibrated (bound) to HSA (50 mM KH_2PO_4 buffer, pH 7.50) and were excited at 320 nm and 263 nm, respectively. The emission spectrum was measured in the range 350 – 500 nm for warfarin and 380 – 450 nm for ibuprofen. The HSA and fluorescence probe concentrations were both used at 5.0 μM. Titrations were performed by increasing the concentrations of **CoL** or **HL** in the protein-probe solution from 0 to 25 μM. Fluorescence emission measurements on DMSO were carried out, and showed there was no emission from DMSO affecting the emission spectra.

1.2. Protein CD spectroscopy

All protein circular dichroism experiments were performed in a similar manner to our previously reported methods [3–5].

Far-UV CD. Far-UV CD spectra of solutions of HSA (1×10^{-6} mol dm^{-3}) in the absence and presence of **HL** (0–20 μM) were recorded with a JASCO J-1500 CD spectrometer equipped with a Peltier temperature controller (37 °C, 50 mM, pH 7.5 KH_2PO_4 buffer). A scan speed of 100 nm min^{-1} was employed for spectral acquisition with a 0.5 nm data pitch and a response time of 2s. Each spectrum was the average of three scans. Spectra were recorded over a wavelength range of 186–260 nm (1 cm pathlength quartz cuvette).

Near UV-CD. Near UV-vis CD spectra of solutions of HSA (15×10^{-6} M; 250–310 nm, 50 mM, pH 7.5 KH_2PO_4 buffer) were recorded similarly to detect changes in the tertiary structure of HSA. A scan speed of 100 nm min^{-1} was used with a 0.5 nm data pitch (response time, 2 s); each spectrum was the average of three scans from 250 – 310 nm.

Analysis of CD spectra to determine secondary structure composition. We utilised the JWMVS-529 Protein Secondary Structure Analysis program, incorporated in JASCO's Spectra Manager™ package, to analyse the secondary structure composition of HSA based on the recorded CD spectra. This program employs a library of 26 protein CD spectra (186–260 nm) provided by JASCO to establish a calibration model [7[.By applying the partial least squares (PLS) method and principal component regression (PCR) techniques [8], the experimental CD spectra were fitted to the calibration model, allowing for accurate estimation of the fractional composition of α-helix, β-sheet, turn, and unordered coil structures. Notably, this approach significantly enhances the assessment of β-sheet motifs, which lack strong specific CD marker bands. We opted for these methods over an older algorithm, the JWSSE-513 Protein Secondary Structure Analysis program, offered by JASCO, which employs a classical least squares (CLS) fitting algorithm based on the reference spectra set of [9][6]. Although other methods for protein secondary structure prediction can be found in the literature, we did not utilize them in this study as suitable methods were readily available in JASCO's Spectra Manager™ package on the spectrometer's controlling computer [10, 11].

1.3 Molecular docking and dynamics

Protein docking and MD simulations were performed in a similar manner to our previously reported methods[3]. In brief the methods are highlighted below using various software's employed in Schrödinger Suite 2022-3.

Ligand Preparation

The LigPrep module of Schrödinger was used to prepare ionization states and geometry-optimized input structures for **HL** using a pH range of 7.4 ± 2.0. The structure of **CoL** used for docking inputs were obtained by DFT simulations at the CAM-B3LYP/LANL2DZ level of theory in a water solvent continuum (SCRF PCM model) and implementing the GD3BJ empirical dispersion energy correction. Minor adjustments were required to prepare the metal chelate structures for docking with GLIDE. Firstly, the Co ion was given a +2 charge and the coordinating oxygen atoms were each given a -1 charge. Secondly, the bonds from the two N-donor and O-donor atoms to the metal ion were assigned bond orders of zero. This step is mandatory as it obviates the need for specific force field parameters involving the metal ion; the coordination geometry is then restrained to remain similar to the input DFT-calculated geometry by GLIDE during optimization and fitting. Lastly, partial charges were assigned to the structures using the OPLS2005 force field with standard parameters for LigPrep (LigPrep, Schrödinger, LLC, New York, NY, 2021-4).

Protein Preparation

The 2.5-Å X-ray crystal structures of HSA in complex with warfarin[7], was retrieved from the Protein Data Bank (PDB ID codes: 1HA2). The structure of HSA was pre-processed, minimized, and refined using the Protein Preparation Wizard[8] employed in Schrödinger Suite 2022-3. This step included eliminating crystallographic waters within 5 Å of the ligand binding site, adding missing hydrogen atoms and side chain

atoms, as well as assigning the appropriate charge and protonation state of the receptor structure (pH = 7.4) using Prime. Finally, the protein structure was subjected to energy minimization using Macromodel[9] and the S-OPLS force-field[10,11] with a RMSD cut-off value of 0.30 Å to resolve steric clashes among closely spaced residues arising from the addition of hydrogen atoms.

Protein Ligand Docking

The prepared ligands were docked into HSA using Glide[12] to identify potential binding sites for the metal chelates on the serum protein. The receptor grid was centred in Sudlow's site I on Trp-214 with dimensions $40 \times 40 \times 40$ Å^3 so that more than 90% of the protein was sampled for potential binding sites. The portions of the protein not included in the receptor grid exceed the >25 Å limit to induce intrinsic fluorescence quenching. Therefore, are not considered potential binding sites. XP(extra precision)[13] docking was used. Because G-scores produced from docking are poorly correlated to experimental data[14], the G-score is not considered when determining a potential binding site. However, the G-score may be used to discriminate ligand poses within a subdomain (binding site). The docked ligands should corroborate the experimental data i.e., fluorescence and CD, even if the G-score is low.

Molecular dynamics: HSA

Molecular dynamics (MD) simulations were conducted on the best-docked DNA-ligand complexes using Desmond[15] and the OPLS2005 force field. Prior to simulation, the DNA-ligand complexes were pre-processed, and the System Builder in Desmond was used to solvate the system with TIP3P[16] water molecules. The biomolecular system was placed in an orthorhombic box with a 5 Å buffer between the box boundary and the DNA-ligand complex, then neutralized with Na^+ as needed. The simulations were run for 100 ns, with approximately 1000 frames recorded at 100 ps intervals. Before starting the simulation, the system was relaxed and equilibrated under the NPT ensemble[17] at 310 K and 1.01 bar. The resulting trajectories were analyzed using Maestro. A caveat is that the Centre of High Performance Computing (CHPC) in South Africa allows the users a maximum of 12 h of Desmond simulation time, therefore, the maximum time we can run a MD simulation for is 100 ns. To ensure the trajectory is reliable and the best one, each simulation is run in triplicates. .

Caveat surrounding the force field limitations in describing metal–ligand bonds

A caveat that must be acknowledged is the limitations of conventional force fields such as OPLS4 in fully describing the covalent and electronic character of metal–ligand interactions. To ensure consistency within the simulation framework, the Co–ligand bond orders were set to zero, allowing the coordination environment to be maintained through nonbonded electrostatic and van der Waals interactions. Partial charges were assigned to both the cobalt ion and the coordinating oxygen atoms to better reproduce the metal's electrostatic field and ligand polarization effects. This approach has been widely employed for metal-containing systems in molecular docking and dynamics simulations where full quantum mechanical parametrization is computationally prohibitive. While such classical models cannot capture charge transfer or orbital mixing effects, they reliably preserve the coordination geometry and relative stability trends, which were the primary focus of this study.

All calculations were performed using the OPLS4 force field in Schrödinger, which provides updated torsional and nonbonded parameters compared to previous versions, improving the robustness of the simulations for metalloprotein and organometallic systems [18,19].

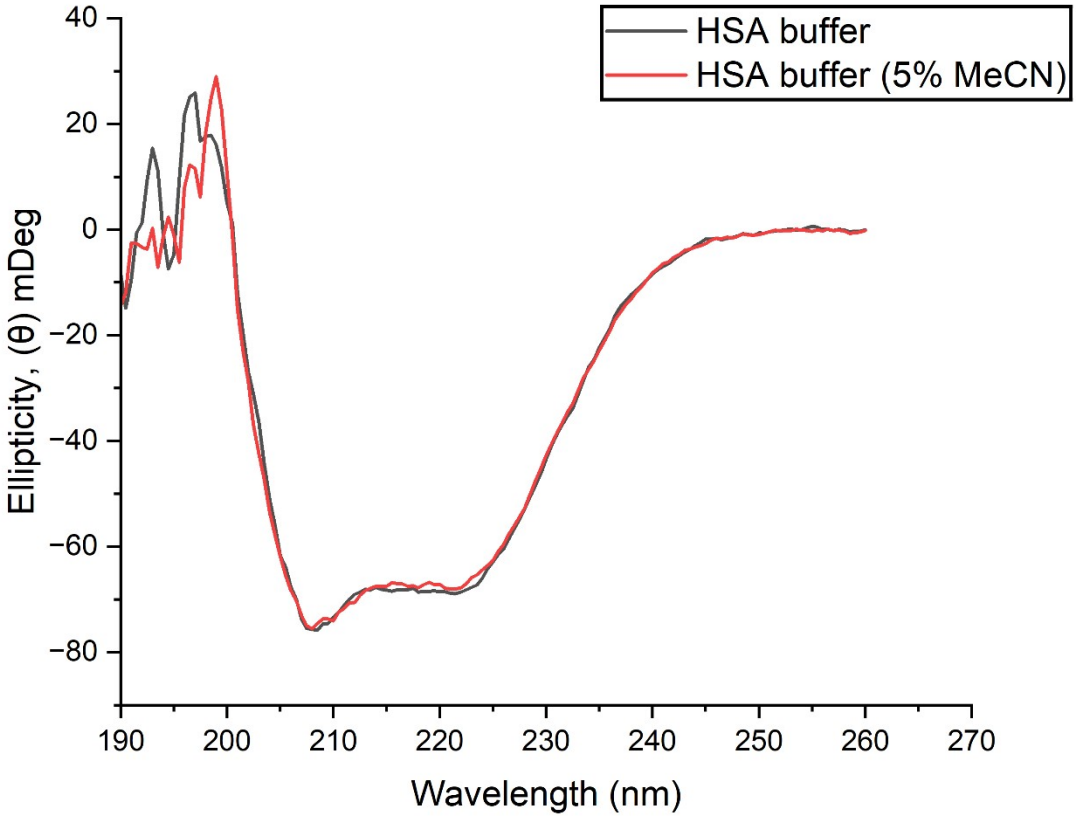

Figure S13. Plots of the far-UV CD spectra of native HSA and the protein incubated with 5% acetonitrile recorded at 310 K in 50 mM KH_2PO_4 buffer at pH 7.5

Table S1 Summary of GLIDE XP docking scores and selected interaction energy parameters for HSA targets prepared from ligand-free structures derived from PDB codes 1HA2. The docking runs were truncated to report only the top-scoring ligand pose for each ligand. All energies are in units of kcal mol^{-1}.

Ligand	XP Gscore	Glide Energy
HL	–4.842	–30.16
CoL	–4.048	–29.01

References

1. van de Weert, M. Fluorescence Quenching to Study Protein-Ligand Binding: Common Errors. *Journal of fluorescence* **2010**, *20*, 625–629.
2. Van de Weert, M.; Stella, L. Fluorescence Quenching and Ligand Binding: A Critical Discussion of a Popular Methodology. *Journal of Molecular Structure* **2011**, *998*, 144–150.
3. Sookai, S.; Bracken, M.L.; Nowakowska, M. Spectroscopic and Computational pH Study of NiII and PdII Pyrrole-Imine Chelates with Human Serum Albumin. *Molecules* **2023**, *28*, 7466.
4. Sookai, S.; Munro, O.Q. Complexities of the Interaction of NiII, PdII and PtII Pyrrole-Imine Chelates with Human Serum Albumin**. *ChemistryEurope* **2023**, *1*, e202300012, doi:10.1002/ceur.202300012.
5. Sookai, S.; Q. Munro, O. Spectroscopic and Computational Study of the Interaction of Pt(Ii) Pyrrole-Imine Chelates with Human Serum Albumin. *Dalton Transactions* **2023**, *52*, 14774–14789, doi:10.1039/D3DT02039H.
6. Yang, J.T.; Wu, C.-S.C.; Martinez, H.M. [11] Calculation of Protein Conformation from Circular Dichroism. In *Methods in Enzymology*; Enzyme Structure Part K; Academic Press, 1986; Vol. 130, pp. 208–269.
7. Petitpas, I.; Bhattacharya, A.A.; Twine, S.; East, M.; Curry, S. Crystal Structure Analysis of Warfarin Binding to Human Serum Albumin: ANATOMY OF DRUG SITE I *. *Journal of Biological Chemistry* **2001**, *276*, 22804–22809, doi:10.1074/jbc.M100575200.
8. Madhavi Sastry, G.; Adzhigirey, M.; Day, T.; Annabhimoju, R.; Sherman, W. Protein and Ligand Preparation: Parameters, Protocols, and Influence on Virtual Screening Enrichments. *J Comput Aided Mol Des* **2013**, *27*, 221–234, doi:10.1007/s10822-013-9644-8.
9. Mohamadi, F.; Richards, N.G.J.; Guida, W.C.; Liskamp, R.; Lipton, M.; Caufield, C.; Chang, G.; Hendrickson, T.; Still, W.C. Macromodel—an Integrated Software System for Modeling Organic and Bioorganic Molecules Using Molecular Mechanics. *J. Comput. Chem.* **1990**, *11*, 440–467, doi:10.1002/jcc.540110405.
10. Jorgensen, W.L.; Tirado-Rives, J. The OPLS [Optimized Potentials for Liquid Simulations] Potential Functions for Proteins, Energy Minimizations for Crystals of Cyclic Peptides and Crambin. *J. Am. Chem. Soc.* **1988**, *110*, 1657–1666.
11. Kaminski, G.A.; Friesner, R.A.; Tirado-Rives, J.; Jorgensen, W.L. Evaluation and Reparametrization of the OPLS-AA Force Field for Proteins via Comparison with Accurate Quantum Chemical Calculations on Peptides. *J. Phys. Chem. B* **2001**, *105*, 6474–6487, doi:10.1021/jp003919d.
12. Friesner, R.A.; Banks, J.L.; Murphy, R.B.; Halgren, T.A.; Klicic, J.J.; Mainz, D.T.; Repasky, M.P.; Knoll, E.H.; Shelley, M.; Perry, J.K.; et al. Glide: A New Approach for Rapid, Accurate Docking and Scoring. 1. Method and Assessment of Docking Accuracy. *J. Med. Chem.* **2004**, *47*, 1739–1749, doi:10.1021/jm0306430.
13. Friesner, R.A.; Murphy, R.B.; Repasky, M.P.; Frye, L.L.; Greenwood, J.R.; Halgren, T.A.; Sanschagrin, P.C.; Mainz, D.T. Extra Precision Glide: Docking and Scoring Incorporating a Model of Hydrophobic Enclosure for Protein−Ligand Complexes. *J. Med. Chem.* **2006**, *49*, 6177–6196, doi:10.1021/jm051256o.

14. Warren, G.L.; Andrews, C.W.; Capelli, A.-M.; Clarke, B.; LaLonde, J.; Lambert, M.H.; Lindvall, M.; Nevins, N.; Semus, S.F.; Senger, S.; et al. A Critical Assessment of Docking Programs and Scoring Functions. *J. Med. Chem.* **2006**, *49*, 5912–5931, doi:10.1021/jm050362n.
15. Bowers, K.J.; Sacerdoti, F.D.; Salmon, J.K.; Shan, Y.; Shaw, D.E.; Chow, E.; Xu, H.; Dror, R.O.; Eastwood, M.P.; Gregersen, B.A.; et al. Molecular Dynamics---Scalable Algorithms for Molecular Dynamics Simulations on Commodity Clusters. In Proceedings of the Proceedings of the 2006 ACM/IEEE conference on Supercomputing - SC '06; ACM Press: Tampa, Florida, 2006; p. 84.
16. Jorgensen, W.L.; Chandrasekhar, J.; Madura, J.D.; Impey, R.W.; Klein, M.L. Comparison of Simple Potential Functions for Simulating Liquid Water. *The Journal of chemical physics* **1983**, *79*, 926–935.
17. Jorgensen, W.L. Convergence of Monte Carlo Simulations of Liquid Water in the NPT Ensemble. *Chemical Physics Letters* **1982**, *92*, 405–410.
18. Lu, C.; Wu, C.; Ghoreishi, D.; Chen, W.; Wang, L.; Damm, W.; Ross, G.A.; Dahlgren, M.K.; Russell, E.; Von Bargen, C.D.; et al. OPLS4: Improving Force Field Accuracy on Challenging Regimes of Chemical Space. *J Chem Theory Comput* **2021**, *17*, 4291–4300, doi:10.1021/acs.jctc.1c00302.
19. Monticelli, L.; Tieleman, D.P. Force Fields for Classical Molecular Dynamics. *Methods Mol Biol* **2013**, *924*, 197–213, doi:10.1007/978-1-62703-017-5_8.